IOP Publishing J. Neural Eng. 18 (2021) 056050 https://doi.org/10.1088/1741-2552/ac28d2

Journal of Neural Engineering

OPEN ACCESS

PAPER

Cortical network and connectivity underlying hedonic olfactory perception

Alejandro Luis Callara[1,2,*], **Alberto Greco**[1,2], **Johannes Frasnelli**[3], **Gianluca Rho**[2], **Nicola Vanello**[1,2] and **Enzo Pasquale Scilingo**[1,2]

[1] Research Center 'E. Piaggio', School of Engineering, University of Pisa, Largo Lucio Lazzarino 1, 56122 Pisa, Italy
[2] Dipartimento di Ingegneria dell'Informazione, University of Pisa, Via G. Caruso 16, 56122 Pisa, Italy
[3] Département d'anatomie, Université du Québec à Trois-Rivières, 3351, boul. des Forges, C.P. 500, G9A 5H7 | Local 3439 L.-P, Trois-Rivières, Québec, Canada
* Author to whom any correspondence should be addressed.

E-mail: alejandro.callara@ing.unipi.it

Keywords: EEG, ICA, brain networks, causal interactions, hedonic olfaction, orbitofrontal cortex

RECEIVED 26 November 2020
REVISED 12 August 2021
ACCEPTED FOR PUBLICATION 21 September 2021
PUBLISHED 11 October 2021

Abstract

Objective. The emotional response to olfactory stimuli implies the activation of a complex cascade of events triggered by structures lying in the limbic system. However, little is known about how this activation is projected up to cerebral cortex and how different cortical areas dynamically interact each other. *Approach.* In this study, we acquired EEG from human participants performing a passive odor-perception task with odorants conveying positive, neutral and negative valence. A novel methodological pipeline integrating global field power (GFP), independent component analysis (ICA), dipole source localization was applied to estimate effective connectivity in the challenging scenario of single-trial low-synchronized stimulation. *Main results.* We identified the brain network and the neural paths, elicited at different frequency bands, i.e. $\theta(4-7\text{Hz})$, $\alpha(8-12\text{Hz})$ and $\beta(13-30\text{Hz})$, involved in odor valence processing. This brain network includes the orbitofrontal cortex (OFC), the cingulate gyrus (CgG), the superior temporal gyrus (STG), the posterior cingulate cortex/precuneus (PCC/PCu) and the parahippocampal gyrus (PHG). It was analyzed using a time-varying multivariate autoregressive model to resolve time-frequency causal interactions. Specifically, the OFC acts as the main node for odor perception and evaluation of pleasant and unpleasant stimuli, whereas no specific path was observed for a neutral stimulus. *Significance.* The results introduce new evidences on the role of the OFC during hedonic perception and underpin its specificity during the odor valence assessment. Our findings suggest that, after the odor onset different, bidirectional interactions occur between the OFC and other brain regions associated with emotion recognition/categorization and memory according to the stimulus valence. This outcome unveils how the hedonic olfactory network dynamically changes based on odor valence.

1. Introduction

Processing of multiple streams of information frequently occurs in the orbitofrontal cortex (OFC) [1]. Indeed, several neural pathways convey information from the ventral (or object) visual stream, taste, olfactory and somatosensory areas to the OFC, as well as in the other direction [2]. Functional MRI and other imaging techniques showed that amongst other tasks the OFC evaluates the valence of olfactory stimuli (i.e. pleasantness/ unpleasantness) [3, 4], by interacting with primary olfactory cortex (e.g. the piriform cortex) and other structures [5–9]. Yet, the cortical dynamics during and after olfactory stimulation cannot be described when using fMRI, due to its poor temporal resolution. In turn, EEG has an unmatched high temporal resolution and thus the potential to unveil cortical interactions underlying odor valence. Nevertheless, so far EEG has mostly been used to characterize the cortical activity involved in olfactory processes by means of spectral power analyses and event-related-potentials (ERPs)

[10–12]. While these techniques allow to identify individual brain areas, they do not permit the investigation of interactions between cortical areas. However, since emotions are elicited over distributed brain networks [13, 14], and because subtle differences in emotional content may selectively activate these networks [15], alternative methods must be used when aiming at understanding the neurobiological underpinning of processing of emotional content. In this context, connectivity measures based on multivariate autoregressive (MVAR) models can provide both the directionality of the interaction between localized brain sources, as well as the frequencies at which such interactions occur [16]. Furthermore, time-varying solutions of these methods enable to describe interactions dynamically [17], making them especially suited for analyzing the temporal cascade of events that follow stimulation. In particular, this methodology found great applicability, ranging from the physiological aspects of network-related disorders, such as Alzheimer's and Parkinson's Disease [18], to the discrimination of BCI-related tasks [19]. However, despite this wide-field of applications, to the best of our knowledge, no previous studies have yet used such techniques to analyze EEG-based effective connectivity during olfactory stimulation.

One of the main challenges in EEG studies with olfactory stimuli is represented by the stimulation paradigm. Specifically, precise stimulus-timing and adequate number of stimuli characterizing the experimental protocol are two factors that majorly affect the observations. The former is required in the analysis of event-related psychophysiological measures, as for instance olfactory ERP, and typically achieved with the use of an olfactometer [20]. The latter relies instead on the trade-off between sufficient inter-stimulus-interval (ISI) between olfactory stimuli [11, 21], required because of habituation, and the duration of the experiment (i.e. the shorter the better). Nevertheless, in many social ecological scenarios the olfactory response arises from single or few stimuli. Furthermore, in such scenarios, a high synchronization among neural responses to olfactory stimuli could be challenging due to difficulties in identifying the precise moment in which the olfactory stimulus is inhaled and therefore perceived. In this context, developing novel methodological approaches for the characterization of olfactory-related EEG dynamics in nonstructured settings would certainly have a relevant impact. To this aim, we propose a new processing pipeline to deal with single-trial low-synchronized olfactory stimuli implementing MVAR models with an ad-hoc sliding-window approach. Indeed, on the one hand, our pipeline is able to foster robust estimates of interactions for single-trial stimuli, taking care of model parameter setup [22]; on the other hand, it limits the impact of low synchronization by smoothing the observed interactions after stimulus administration, due to the sliding-window approach.

Another crucial aspect in the study of the neural correlates of olfaction is related to the close relationship between odors and emotions. In this context, the most basic classification of odors is based on valence and intensity [5]. In particular, exposure to olfactory stimuli evokes a response in specific neural systems that evaluate odor valence and intensity as well as higher order tasks [5, 12]. Intensity is hereby determined by the concentration of the odorant. Valence, however, is not exclusively a consequence of molecular features of the odorant [6], but also the result of perceptual memory established at prior exposure [12]. As a result, odor recognition is the matching of the evoked neural profile to pre-established odor templates [23]. In this context, it has been recently shown that olfactory stimuli of different pleasantness levels can induce changes in functional connectivity among brain modules, and that such changes could be linked to emotional processing [24]. In this view, quantifying the cortico-cortical interactions between brain areas occurring after olfactory stimuli with positive and negative valence may be of particular interest, although they never have been investigated.

In this work, we analyzed EEG acquisitions from healthy subjects performing a passive odor-administration task and investigated the potential and relevant cortico-cortical interactions in mediating odor valence assignment and memory involvement. Specifically, we hypothesized that the exposure to odorants with different valence could trigger interactions among distributed cortical activity. In addition, we attempted at observing potential differences in such interactions based on odor valence. To this aim, we applied a new processing pipeline designed ad-hoc for studying cortico-cortical causal interactions in the challenging scenario of single trial stimulation without the use of a computer controlled olfactometer (i.e. by presenting odors in bottles). Accordingly, we first performed independent component (IC) analysis (ICA, [25]) of EEG signals at the subject level, in order to exploit the instantaneous temporal independence of IC, limiting zero-lag effects on the subsequent MVAR model estimation [26, 27]. Then, subject-specific IC were clustered at the group level with a K-means algorithm, in order to identify common brain activity across subjects. Specifically, the equivalent current dipoles [28] associated with ICA maps were clustered based on their position, guaranteeing homogeneous spatial localization among clusters. Afterwards, time-series associated with network nodes were used to construct MVAR models from which the renormalized partial directed coherence (RPDC) was derived [29]. Such normalization of MVAR model coefficients is a scale-free measure that allows for direct comparison of causalities across subjects. Patterns of causal interaction were estimated for olfactory stimuli of

different valence (pleasant, neutral, unpleasant). The analysis was confined to a 15 s-long time-window ranging from 5 s before the stimulus presentation to 10 s after. The window duration was inferred from a time-varying global field power (GFP, [30]) analysis. Specifically, we identified those time-windows during which significant changes in GFP were observed with respect to a resting baseline. In such windows, we then analyzed time-varying causal interactions with a moving-window approach, controlling the local stationary of signals that is required for stable MVAR estimation. Rigorous statistical surrogate testing allowed us to identify the amount of interaction among the clustered sources even with a limited number of stimuli. The experimental paradigm of odor administration was designed taking into account a sufficient inter-stimulus interval to recover the baseline (i.e. 60 s) [11, 21] and sufficient stimulus duration [31–33]. The perceived valence of the stimuli was controlled by the self-assessment-manikin (SAM) test [34].

2. Materials and methods

2.1. Participants

The experimental protocol was approved by the Ethical Committee of the University of Pisa. All participants signed an informed consent prior to the experiment.

We recruited 30 healthy volunteers (age 26 ± 2, 16 males, all right-handed) for this study. We asked participants not to smoke, to eat or to drink in the 30 min preceding the experiment. We also asked them not to use any deodorant nor perfume limiting any possible interference with the experiment. We determined olfactory threshold by preparing ten solutions diluting a mother solution of N-butanol ($CH_3CH_2CH_2CH_2OH$; 4.05 g L^{-1}) according to increasing powers of two (8-4096), we asked each participant to identify the N-butanol solution with respect to distilled water. For each participant, we considered the test to be successfully concluded after four consecutive correct distinctions of N-butanol with respect to distilled water. All 30 participants had similar olfactory perception threshold ensuring a homogeneous panel in terms of olfactory perception [21].

2.2. Stimuli

We administered five different odorants, namely (a) vanillin ($C_8H_8O_3$; 152.15 g mol^{-1}); (b) benzaldehyde (C_6H_5CHO; 106.12 g mol^{-1}); (c) N-butanol ($CH_3CH_2CH_2CH_2OH$; 74.12 g mol^{-1}); (d) isovaleric acid ($(CH_3)_2CHCH_2COOH$; 102.13 g mol^{-1}); (e) butyric acid ($CH_3CH_2CH_2CO_2H$; 88.11 g mol^{-1}). We selected odorants in order to convey positive valence (vanillin, benzaldehyde) and negative valence (isovaleric acid, butyric acid) [35]. We chose odorant concentrations to guarantee isointense solutions, and we kept odorants into separate vials. We administered odor stimuli by approaching vials at ∼2 cm from participants' nostrils. Each stimulus was administered once.

2.3. Experimental protocol

Participants followed this protocol: (a) 3 min of initial rest; (b) 1 min of pre-stimulus rest; (c) 5 s of olfactory stimulation; (d) 1 min of post-stimulus rest; (e) self-assessment questionnaire. The duration of the stimulation was chosen based on previous works using similar stimulation lengths [31–33]. We repeated this block for each odorant. The order of stimuli was randomized across subjects. After each administration, participants scored the stimulus in terms of arousal (from 1 to 5) and valence (from −2 to 2) according to the Self-Assessment Manikin (SAM) test [34]. Participants kept their eyes closed during the experiment in order to exclude visual stimulation and other type of interference (e.g. expectation, anticipation) while approaching the vials to their noses. They sit on a chair in an isolated room. Participants were not instructed to perform any particular breathing/sniffing technique, instead they breathe normally during the experiment.

2.4. EEG acquisition setup

We recorded the EEG signal with a 128-channel Geodesic EEG System 300 from Electrical Geodesics, Inc. (EGI). Electrodes were grounded/referenced through two additional channels placed between Cz and Pz, and in the vertex of the cap (i.e. Cz), respectively. We maintained impedance of each electrode below 20 $k\Omega$ during all acquisitions. We acquired EEG signal with a sampling frequency of 500 Hz.

2.4.1. EEG analysis

We preprocessed the EEG signals using EEGLAB [36]. First, we filtered EEG data with a zero-phase anti-aliasing filter and then down sampled to a sampling frequency of 100 Hz. We then high-pass filtered data above 1 Hz with a non-causal filter to improve stationary without affecting signal phase [37]. Next, we cleaned EEG with an optimized adaptive PCA-based spatial filter removing high-amplitude components (e.g. eye-blinks, muscle, sensor motion) [38, 39]. We then visually inspected preprocessed data to eventually remove parts of the data not properly cleaned by the spatial filter. More than the 92.74% of the original data was retained. Finally, we average-referenced EEG signals and decomposed them into sets of maximally independent components (ICs) with the AMICA algorithm [40]. These ICs reflected both brain sources and different types of artifacts (muscular, ocular and other sources of noise). Six participants were excluded from further analysis due to low EEG signal quality resulting in data from 24 participants to be included in the subsequent analysis.

2.5. IC selection and network identification

To identify non-brain sources of activity we applied a semi-automatic procedure. First, we used the FieldTrip [28] to model each independent component as an equivalent current dipole within a boundary element model of the head based on the template from Montreal Neurological Institute (MNI; Montreal, Canada). We estimated each dipole with a two-stage procedure. First, we obtained a coarse localization on a fixed three-dimensional grid. The origin of Cartesian axes was placed in correspondence of the MNI origin (i.e. the anterior commissure), while the X, Y and Z axes extended left-right, posterior-anterior and inferior-superior, respectively. The grid consisted of 34 equally spaced points ranging -85 to $+85$ mm in the X and Y direction, while 17 points were used between 0 and $+85$ mm in the Z direction. Among all the grid points, we restricted dipoles reconstruction to only gray matter positions based on a segmentation of the MNI template. Then, we performed a nonlinear optimization of dipole position and orientation by minimizing the error between the model and the measured potential [28]. We excluded from the analysis those components whose best-fit dipole residual variance was higher than the 15% of the scalp map current distribution, since they are likely to be associated with non-brain activity [41]. Finally, we carried out a visual inspection in order to exclude those components whose map, time-course and/or spectrum were associated with artifacts.

We aggregated the remaining components across all subjects and clustered with a K-means algorithm whose feature vector was made of dipole position and orientation. In particular, this was suggested as a convenient way to assess the spatial homogeneity of a set of ICs from a group of subjects [42]. Accordingly, we run K-means with $n = 100$ replicates for reliability purposes. Specifically, since for running K-means algorithm the number of clusters needs to be specified *a priori*, we determined the optimal number of clusters with the silhouette approach [43]. Then, we considered only those clusters that had a contribution from all subjects [42]. In particular, we assumed that these clusters were likely to reflect shared sources among subjects during the experiment. As a result, three additional participants that did not contribute to every cluster were excluded from further analyses. Therefore, data from a total of 21 participants entered analysis.

2.6. GFP analysis

For each stimulus, we estimated GFP ([30]) with a moving-window approach in the range from -5 s to $+15$ s around odor administration. Moving windows were 5 s long and the step between successive windows was 1 s, for a total of 16 windows. The first window covered the last 5 s of the resting state before the onset of the stimulus (i.e. rest condition), while the following segments represented the evolution over time of the GFP after the odor administration. We calculated statistically significant deviations from the rest condition during the odor administration by comparing the GFP of each window with the rest condition with a Wilcoxon sign-rank test (for more details see Statistical analysis section).

2.7. Causality analysis

We estimated network ICs interactions through MVAR modeling of their associated time courses in a time-span ranging from -5 s to $+10$ s around each stimulus onset. We derived MVAR models by means of the Vieira-Morf algorithm, using a moving-window of 5 s and a step of 1 s. We estimated model order by weighting different optimal model orders according to four information criteria (i.e. AIC, BIC, FPE, HQ). We assured validation of the models by testing the whiteness of residuals, the model consistency and stability [26, 44, 45]. Finally, we estimated causal interactions between network ICs on validated models by means of the renormalized partial directed coherence (RPDC) estimator, providing an index of coupling that does not depend on the scale of signals [29]. We evaluated this metrics for each MVAR model yielding to a time-frequency connectivity matrix of RPDC where each column represented a source (FROM) and a sink (TO) node respectively.

2.8. Statistical analysis

In order to assess at the group level how stimulus perception differed, we performed a Wilcoxon test followed by a multiple-comparison correction with Bonferroni method on SAM test scores of intensity and valence. We estimated statistically significant GFP differences between each moving window and the rest condition at the group level through a sign rank Wilcoxon test. We controlled false discovery rate through the Benjamini-Yekuteli correction for multiple testing under dependency [46]. We assessed statistical significance of connectivity estimates by means of a phase randomization approach [47]. We performed 300 randomizations per participant and stimulus. We carried out group level analysis by averaging surrogate distributions from each participant. We averaged for each connection, frequency and time-window separately, i.e. for each (i,j,ω,t). We obtained causality statistical significance by comparing average connectivity across subjects with the group-level null-distribution. We controlled for multiple testing with the false discovery rate procedure presented in [48]. Tests were considered significant whether $p < 0.05$.

3. Results

Participants categorized all odorants equally in terms of intensity, while significant differences were found in terms of valence as shown in figure 1 ($p < 0.05$,

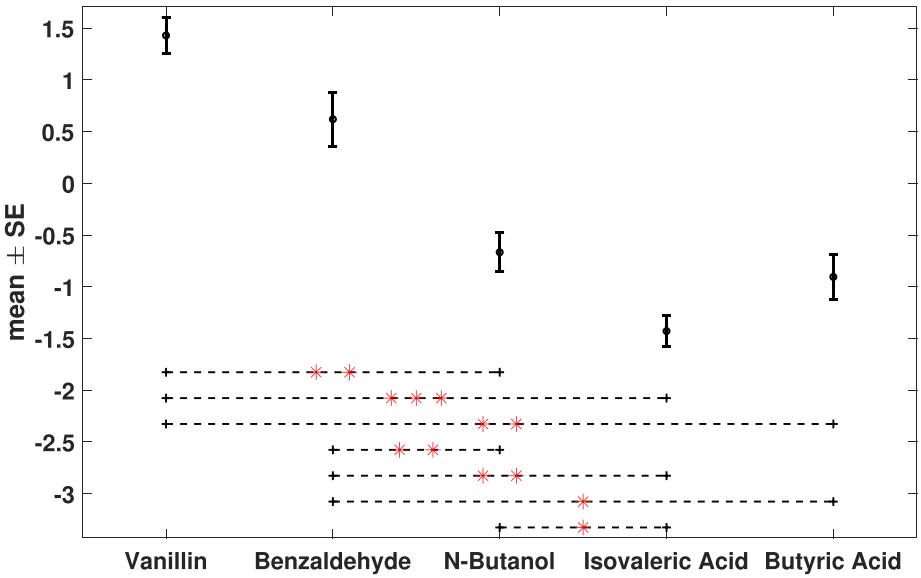

Figure 1. Valence average ± standard error (SE) according to the SAM questionnaire. Significant statistical differences between stimuli are reported ($p < 0.05$, Bonferroni-corrected).

Bonferroni-corrected). We expected vanillin and benzaldehyde to be pleasant, N-butanol to be neutral and isovaleric acid as well as butyric acid to be unpleasant. In fact, participants evaluated vanillin and benzaldehyde as significantly more pleasant than butanol; and isovaleric acid significantly less pleasant than butanol. We did not find any difference between butyric acid and the neutral odor. For the remainder of the study, we therefore selected the most pleasant odor ($O+$) vanillin, the most unpleasant odor ($O-$) isovaleric acid and N-butanol as a neutral reference ($O\#$).

3.1. GFP

We used changes in GFP to define the time-window of interest for the causality analysis. GFP corresponds to the spatial standard deviation, and it quantifies the amount of activity at each time point in the field considering the data from all recording electrodes simultaneously, resulting in a reference-independent descriptor of the potential field [30]. This is particularly useful for defining the timing of relevant changes in brain activity when there is no hypothesis on the spatial location of sources contributing to such changes. Here, we attempted at observing variations in GFP median values before, during and after the stimulus presentation. Based on the observed variations, we identified the time-range of interest for the subsequent connectivity analysis.

We evaluated the evolution of GFP during stimulus administration within 5 s windows ranging from -5 s to $+10$ s with a step size of 1 s (for methodological details see section 2). In particular, the first window, representing the rest condition, was compared with each of the successive windows. We observed significant changes ($p < 0.05$, Bonferroni-corrected) in GFP values during the stimulus administration (figure 2). Specifically, regardless of the stimuli, a decrease in GFP at stimulus onset ($t = 0$) was evident (figure 2). While the time-windows in which this happens are different for each stimulus, all stimuli showed differences around stimulus administration from window $(-1,4)$s to window $(4,9)$s. Accordingly, we performed connectivity analysis from the resting condition $(-5,0)$s to the end of the stimulation $(5,10)$s.

3.2. Network identification and EEG causal interactions

We investigated causal cortico-cortical interactions by means of MVAR modeling of independent components obtained through ICA [25]. Accordingly, we first identified a common network at the group level reflecting the same neural activity across subjects and then analyzed the time-varying causal interactions between network nodes time-series through the RPDC ([29]) estimator, a Granger-based causality measure (methodological details at section 2). Granger-Causality measures are a family of connectivity metrics whose principle of causality is based on temporal precedence. Accordingly, if the prediction error of a time series is reduced by including another time series in the MVAR regression model, then the second series is said to have a causal influence on the first time series. Such causal measures are particularly attractive for EEG analysis since they can be also represented in the frequency domain, and thus giving not only the strength and the direction of the interaction, but also the frequency range at which the interaction is happening.

We identified an average of 120 components per subject, for a grand total of 2523 components. For

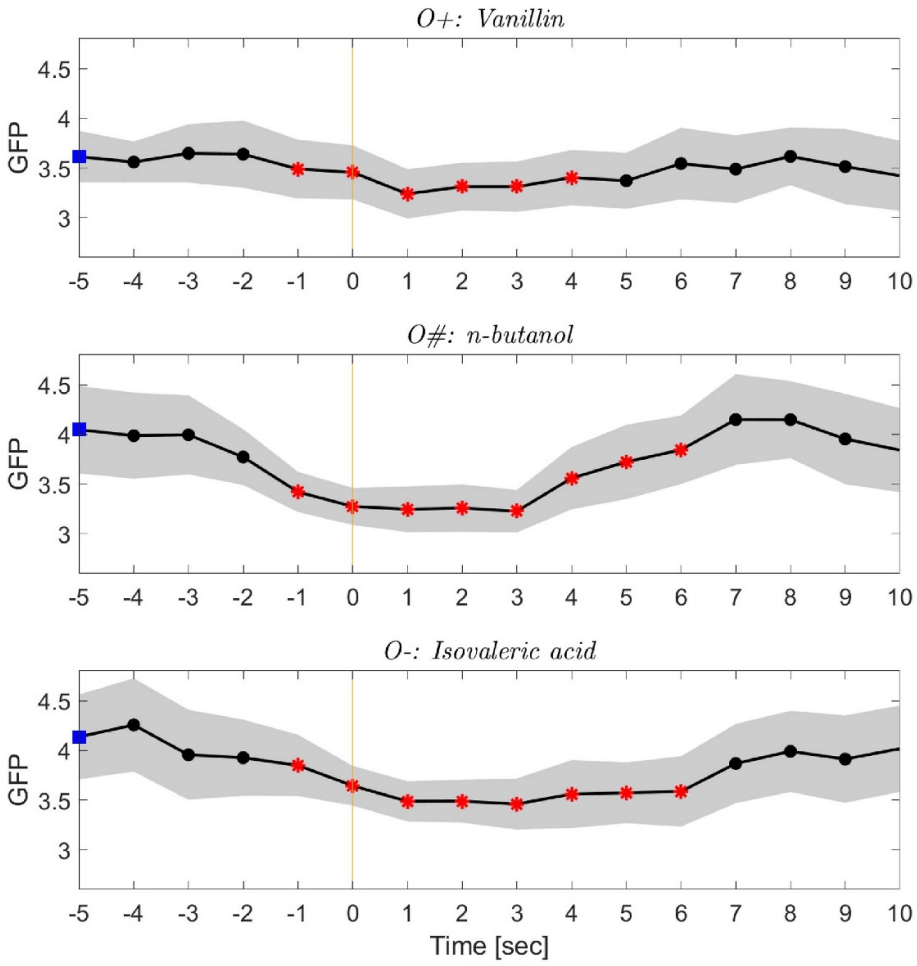

Figure 2. Median ± MAD of GFP between –5 s and +10 s around stimulus onset. Each time-point represent a 5 s-long window. The time-point reported in the horizontal axis represent the starting point of each window. Statistically significant differences between each window and the first window (■) are highlighted with red stars (*)($p < 0.05$, FDR-corrected).

each subject, an average of 15 ICs was associated with non-artefacted activity according to the scalp-map explained-variance of their associated equivalent dipole. We performed K-means clustering with an optimal number of five clusters, according to the silhouette approach. The cluster vector contained three values describing the dipole position and three values describing the orientation, ensuring a homogeneous spatial distribution of the clustered activity and depicting a common network among subjects on which the connectivity analysis was carried out (figure 3 summarizes the identified network across all subjects). Specifically, the network was obtained by clustering all the non-artefactual ICs into an optimal number of clusters (N = 5, estimated with the silhouette approach [43]) through K-means algorithm. We labelled network nodes based on the nearest grey matter to the anatomical position of the cluster centroids according to their $x-y-z$ MNI-coordinates, i.e. precuneus (Cl1: PCC/PCu, (−10,−51,23)), cingulate gyrus (Cl2: CgG (−5,7,25)), orbitofrontal cortex (Cl3: OFC (0,29,−12)), superior temporal gyrus (Cl4: STG (40,−52,14)), and parahippocampal gyrus (Cl5: PHG (−25,−19,−18)).

The causality analysis evidenced significant interactions in the θ, α and β bands during $O+$ and $O-$ ($p < 0.05$, FDR corrected), whereas no significant causality was observed during the neutral stimulus. The spectro-temporal matrices of interactions during $O+$ and $O-$ are shown in figure 4. In particular, we report the time-frequency representation of RPDC(ω, t) for each connection from source nodes (j) (i.e. columns) to sink nodes (i) (i.e. rows). The reported values are averaged RPDC estimates that significantly differed from 0 ($p < 0.05$, FDR corrected) according to the phase randomization surrogate test. We observed that before stimulus presentation, there was no significant interaction. This result indicates that during rest (i.e. baseline), the brain regions contributing to the network are not engaged in any specific interaction among them. Then, after the stimulus presentation, several causal interactions were observed, mainly in the θ, α and β bands. Interestingly, the first time-window with significant connectivity was the one covering the 5 s of stimulus presentation. This happened for both $O+$ and $O-$, whereas for $O\#$ there was not any significant interaction, suggesting that the interactions between

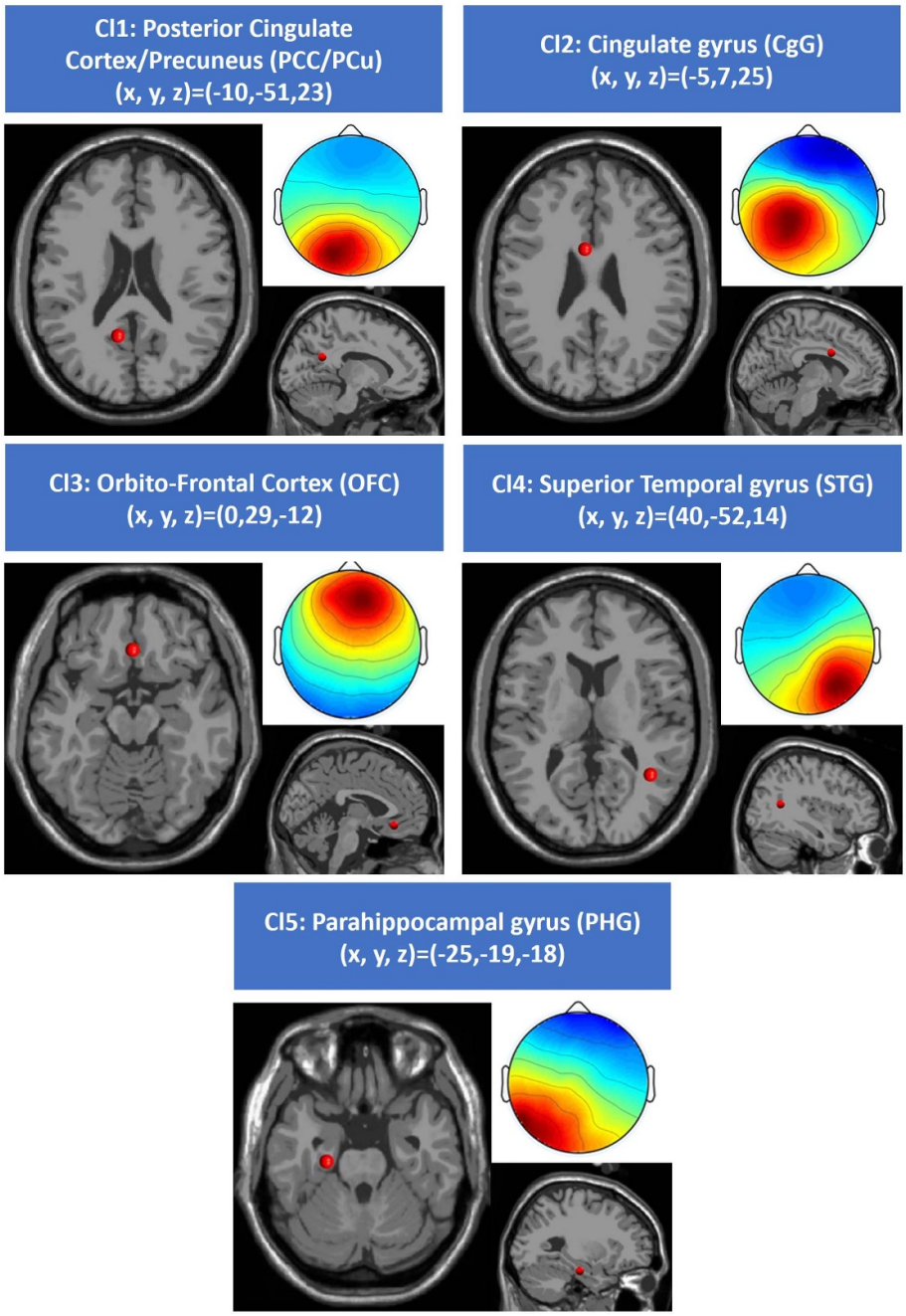

Figure 3. Clustering outcome across all subjects. IC dipole centroid locations in each cluster are displayed in red on a standard MRI atlas. The scalp maps are obtained by averaging single subject scalp maps contributing to the cluster. The cluster centroid positions are anatomically labeled with the closest grey matter according to MNI-coordinates.

network nodes respond to the valence's absolute value, independent of direction.

A three-dimensional rendering of network interactions is shown in figures 5–7. Specifically, for each time-window and each frequency bin we derive a 3D representation of connectivity estimation. Here, we report the RPDC values integrated over three different frequency bands (i.e. θ in figure 5, α in figure 6 and β in figure 7) and for 3 different time-windows. The first window covers from -6.5 s to 0 s and represents the rest condition, while the second and third windows range from 0 s to $+6.5$ s (i.e. the stimulus condition) and from 5 s to 11.5 s (i.e. the post-stimulus condition), respectively. By evaluating network interactions in these three time-windows we show the transitional dynamic before, during, and after the stimuli.

Considering the θ band, we observed that during the stimulus administration the OFC represented the most active node for both stimuli, becoming inactive after the stimulus. However, the interactions were different for $O+$ and $O-$. During $O+$ administration, the OFC received causal inflow from the PHG and produced causal outflow towards the STG, while during $O-$, the OFC interacted only with the CgG (i.e. OFC $\rightarrow$ CgG). Interestingly, during the post-stimulus window, the same three nodes were engaged for both stimuli (i.e. PCC/PCu, STG, CgG).

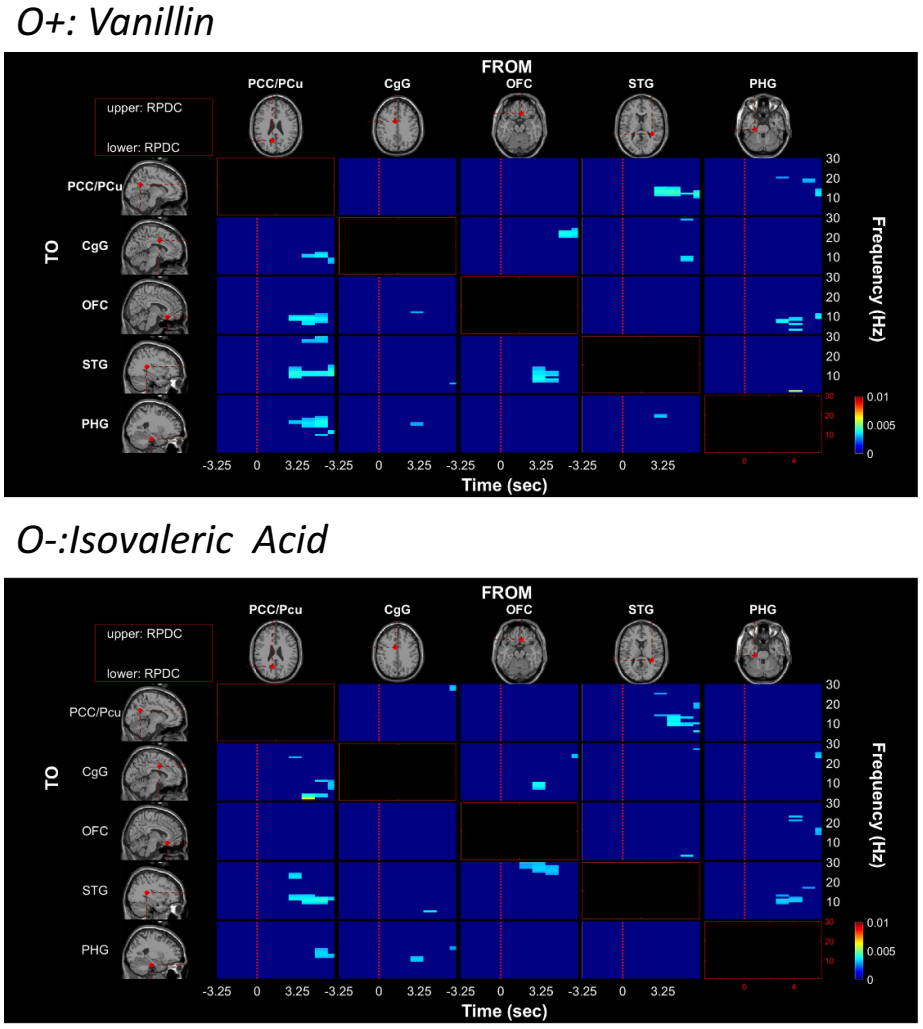

Figure 4. Time-frequency representation of asymmetric cortical connectivity matrix for O+: Vanillin, (top) and O–: Isovaleric Acid, (bottom). Columns represent network sources whereas rows represent network sinks. The dynamic causal interactions around stimulus onset between each source and sink is expressed by the corresponding RPDC matrix. Non-zero causality is reported only for those cases in which $p < 0.05$, and thus only statistically significant causalities are displayed.

A similar behavior was observed also in the α band (figure 6). Specifically, during $O+$ administration, the OFC node represented one of the most active nodes of the network, in being the node with greatest inflow. On the other hand, the PCC/PCu was observed to be the node with higher outflow. Considering $O-$, OFC $\rightarrow$ CgG interactions were present as for the θ band. However, other interactions were present as well (i.e. CgG $\rightarrow$ PHG, PCC/PCu $\rightarrow$ STG, PHG $\rightarrow$ STG). Finally, during the post-stimulus very similar network interactions were observed for both stimuli, with PCC/PCu being the most active node, communicating with PHG, CgG, STG.

In the β band, interactions were more widespread, involving all network nodes during both stimulus and post-stimulus conditions. During the stimulus condition, for both $O+$ and $O-$, similar interactions were present: i.e. PCC/PCu $\rightarrow$ STG, OFC $\rightarrow$ STG, STG $\rightarrow$ PCC/PCu, STG $\rightarrow$ PHG and PHG $\rightarrow$ STG. On the other hand, during the post-stimulus, shared patterns were less compared to stimulus condition and limited to OFC $\rightarrow$ CgG and STG $\rightarrow$ PCC/PCu.

Causality was derived from MVAR model coefficients according to the normalization procedure presented in [29]. MVAR model fitting was performed with an average model order $p = 12$ for each condition (see section 2 for methodological details). In order to ensure a well-posed MVAR estimation (i.e. a datapoint-to-parameter ratio $\geqslant 10$) [22], the moving-window length was adjusted to 6.5 s. Indeed, this represent a major issue for obtaining robust estimates of MVAR model coefficients [22]. Accordingly, we adapted the window length to fulfil the condition $(M\Delta TF_s m)/(M^2 p) \geqslant 10$, where M is the number of network nodes (i.e. $M = 5$), ΔT is the window length (i.e. $\Delta T = 6.5$ s), F_s is the sampling rate (i.e. $F_s = 100$), and m is the number of trials. Thus, in the case of single trials (i.e. $m = 1$) it reduces to $(\Delta TF_s)/(Mp) \geqslant 10$ [22]. For each subject, for each stimulus and for each moving-window, the validation of estimated models evidenced the absence of correlated residuals through the ACF test ($p < 0.05$), suggesting a proper modeling of the underlying dynamics. Average model consistency across subjects was

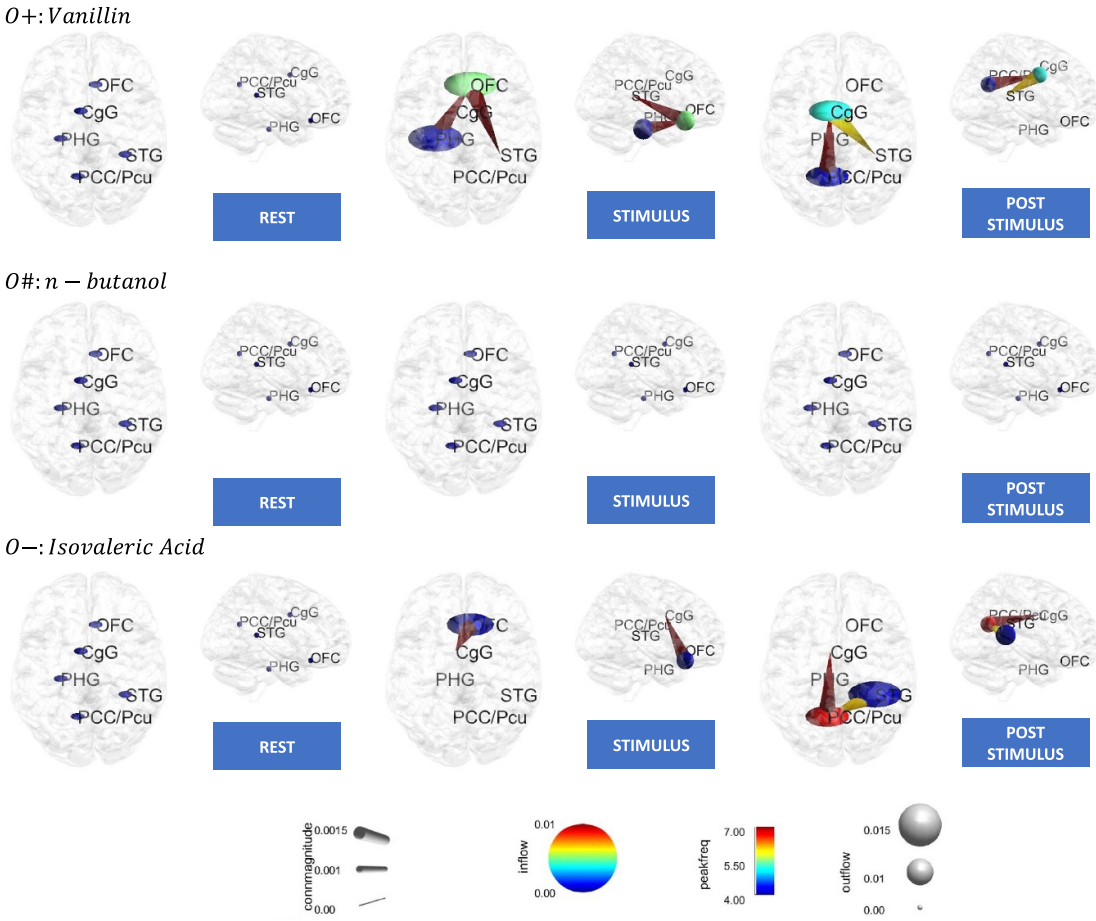

Figure 5. 3D rendering of observed significant causalities during the olfactory stimulation task integrated in the θ band. From left to right the causality profiles for the rest, stimulus, and post-stimulus frames are reported for the positive (i.e. $O+$: vanillin, top), the neutral (i.e. $O\#$: n-butanol, middle) and negative (i.e. $O-$: isovaleric acid, bottom) stimuli. Each network node is reported within a standard template along with its label (i.e. PCC/PCu, CgG, OFC, STG, PHG). Node color and size represent node inflow and outflow, respectively. Edge color represents the frequency at which the peak of connectivity occurs. The connections between network nodes are represented by cylinder of different size, whose magnitude is proportional to connectivity magnitude. The directionality of the connection is given by the direction in which the cylinder tapers. 3D rendering available from the SIFT toolbox [49]. During the stimulus condition the OFC node represent the main driver of the network for both stimuli in the θ band.

91.24% for stimulus $O+$, 93.31% for stimulus $O\#$ and 93.33% for stimulus $O-$. All models were stable according to the maximum eigenvalue criterion [26].

4. Discussion

In this work, we developed a pipeline of analysis for the study of EEG-based brain connectivity during hedonic olfactory stimulation. In particular, we propose a framework that allows to obtain physiologically plausible interactions among brain regions in the presence of single trial stimulation and with a relatively simple stimulation paradigm, in which odors were presented by approaching vials to subjects nose [20]. Twenty-one subjects with comparable olfactory sensitivity participated in an experimental protocol where EEG was monitored during the administration of a pleasant, an unpleasant, and a neutral odor of similar intensity. We show that during stimulation with the pleasant and the unpleasant odor, but not with the neutral odor, the OFC interacts, mainly in the θ and α bands, with several brain regions associated with episodic memory retrieval (i.e. PCC/PCu [50]) and emotional memory (i.e. CgG [51], PHG [52]). In addition, connectivity profiles depended on the direction of odor valence, as different paths were observed for the pleasant and the unpleasant odorant. The causality analysis among IC time-courses allowed us to observe significant differences at the group level in brain interactions based on the hedonic content of different olfactory stimuli. We hypothesized that the higher order processing of non-neutral olfactory stimulation results in differing connectivity networks. In line with this, we observed that both the pleasant and the unpleasant odors produced significant changes in cortico-cortical interactions after stimulus administration. In contrast, we did not observe any significant change in causalities after administration of the neutral stimulus. Similarly, a recent work by Abbasi and colleagues suggested that connectivity differences may arise based on the pleasantness level of positive-valenced olfactory stimuli [24].

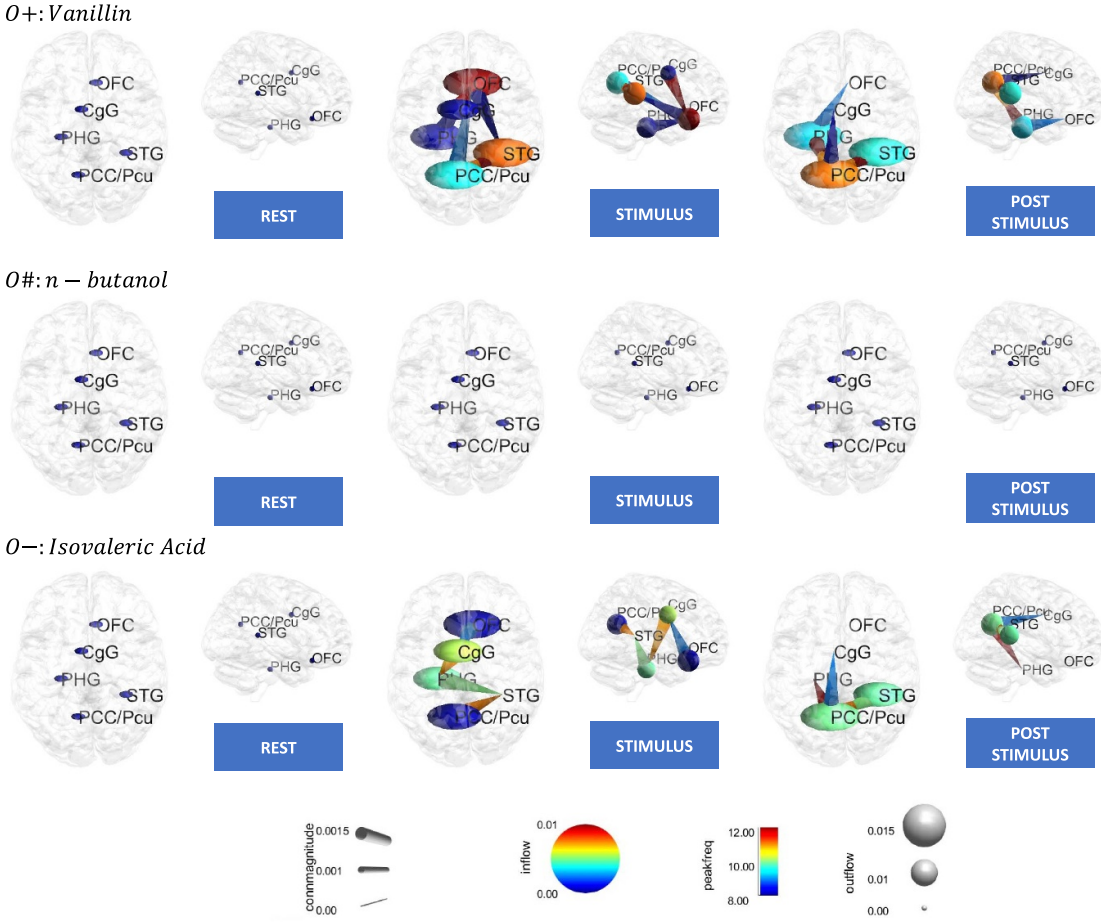

Figure 6. 3D rendering of observed significant causalities during the olfactory stimulation task integrated in the α band. From left to right the causality profiles for the rest, stimulus, and post-stimulus frames are reported for the positive (i.e. $O+$: vanillin, top), the neutral (i.e. $O\#$: n-butanol, middle) and negative (i.e. $O-$: isovaleric acid, bottom) stimuli. Each network node is reported within a standard template along with its label (i.e. PCC/PCu, CgG, OFC, STG, PHG). Node color and size represent node inflow and outflow, respectively. Edge color represents the frequency at which the peak of connectivity occurs. The connections between network nodes are represented by cylinder of different size, whose magnitude is proportional to connectivity magnitude. The directionality of the connection is given by the direction in which the cylinder tapers. 3D rendering available from the SIFT toolbox [49]. In the α band interactions were less specific with respect to the θ band. Nevertheless, also in this case the OFC was one of the most active nodes contributing to the network during the stimulus condition.

Accordingly, based on our results, we can reinforce the hypothesis that the high hedonic content of the non-neutral odors may activate a cascade of events not triggered with a neutral stimulus. This is despite the fact that all stimuli, including the neutral one, induced a change in GFP, in line with the observation that all odorants evoke a cortical response [53].

We estimated causalities at the group level with a multi-step procedure involving (a) independent component analysis of EEG signals, (b) components clustering at the group level, and (c) modeling of IC time-courses with MVAR models, from which the RPDC measure was derived. The network nodes associated with IC time-courses were located in regions associated with emotion processing and memory retrieval and modulation [1, 15]. Specifically, the OFC represented the node with highest inflow during olfactory stimulation, confirming its central role in olfactory perception [2, 54]. Furthermore, the interactions of OFC with other brain areas associated with emotion perception and memory (i.e. PCC/PCu, CgG, PHG, STG)[15, 51, 55] suggest the presence of a distributed network engaged in valence of olfactory processing rather than segregated activations [15]. This is particularly evident in the θ band during the administration of $O+$ where interactions originate in the PHG, project to the OFC, and further to the STG. Interestingly, some of these regions share common networks with the OFC and the amygdala, a center for emotional learning and memory modulation [56]. Another interaction of interest is the PHG-OFC, since the PHG provides the access route for the OFC to the hippocampus, a structure that receives direct input from the olfactory bulb and encodes long-term memory. These pathways may be important for enhanced memory encoding of emotionally salient stimuli [52].

In this study we tested the hypothesis that hedonic content differentially activates common brain networks [15]. Indeed, during $O-$ stimulation fewer

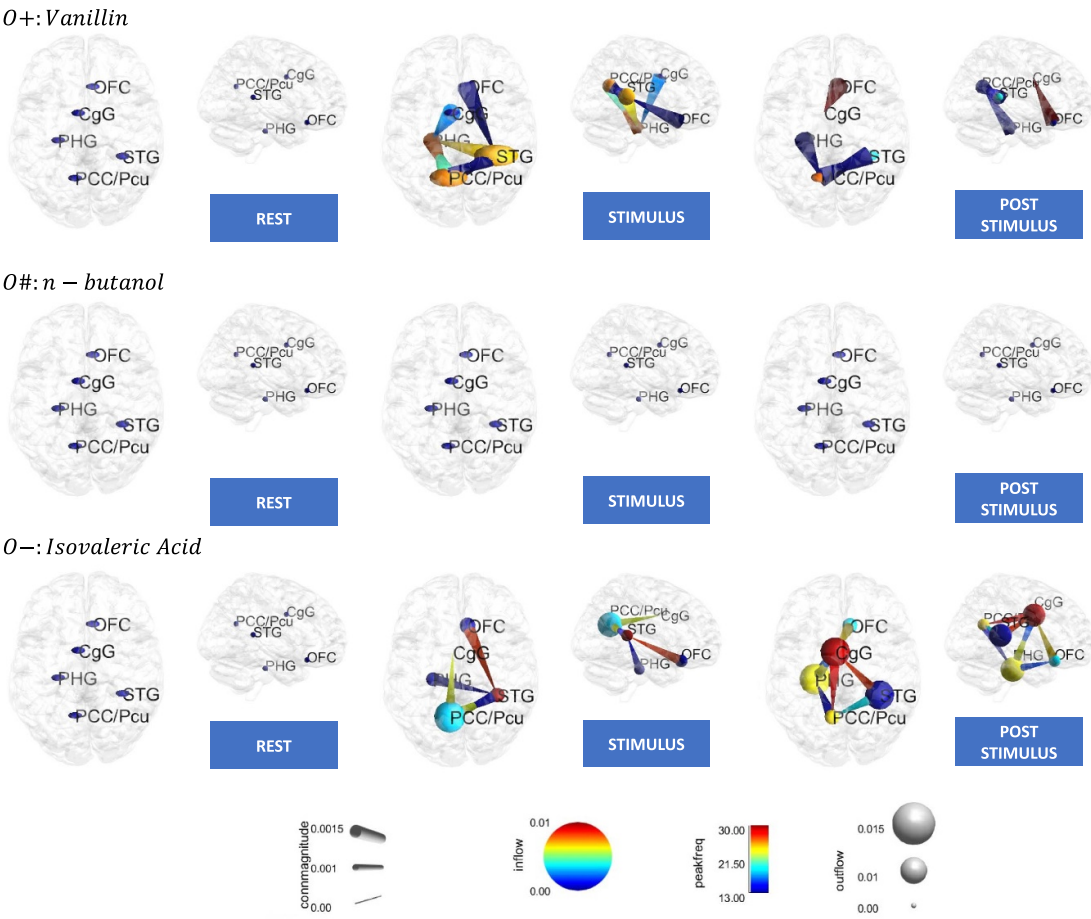

Figure 7. 3D rendering of observed significant causalities during the olfactory stimulation task integrated in the β band. From left to right the causality profiles for the rest, stimulus, and post-stimulus frames are reported for the positive (i.e. $O+$: vanillin, top), the neutral (i.e. $O\#$: n-butanol, middle) and negative (i.e. $O-$: isovaleric acid, bottom) stimuli. Each network node is reported within a standard template along with its label (i.e. PCC/PCu, CgG, OFC, STG, PHG). Node color and size represent node inflow and outflow, respectively. Edge color represents the frequency at which the peak of connectivity occurs. The connections between network nodes are represented by cylinder of different size, whose magnitude is proportional to connectivity magnitude. The directionality of the connection is given by the direction in which the cylinder tapers. 3D rendering available from the SIFT toolbox [49]. In the β band, interactions were more widespread compared to the θ and α bands. In this case, the positive and the negative stimulus induced similar interactions, mainly during the stimulus condition: i.e. PCC/PCu $\rightarrow$ STG, OFC $\rightarrow$ STG, STG $\rightarrow$ PCC/PCu, STG $\rightarrow$ PHG and PHG $\rightarrow$ STG.

interactions occurred compared to $O+$. In addition, $O-$ stimulation evoked only OFC to CgG causalities, highlighting a less interconnected network, again compared to $O+$. For $O-$, CgG is involved in negative affect and may therefore provide an alternative access route to the hippocampus [57–59].

It is worthwhile pointing out that several interactions occurred within the θ and the α bands. Noticeably, these frequency ranges have been widely reported in the cortical changes related to olfactory stimulation [60]. In particular, the θ band has been associated with emotion classification [61] and response-to-odor by evaluating the cortical changes of EEG signal [53]. We can suppose that this frequency range is involved in brain interactions rather than in the activation of single neuron ensembles. Interestingly, OFC dynamical causal interactions come up with the stimulus presentation and disappear after five seconds from the stimulus onset.

Relevant dynamics were observed also in the α band. Indeed, while during the rest condition we did not observe any significant interaction, after the stimulus administration significant interactions were present. Accordingly, we can assume that the olfactory stimulation produced significant changes in network interactions also for this frequency range with respect to the resting baseline. Here, causal interactions were more widespread and more interconnected with respect to the θ band. While in the θ band the OFC played a relevant role in the interaction network only during stimulation; in the α band this contribution was present after stimulation finished, but only for the positive stimulus. This last observation may be due to a longer lasting effect of positive vs. negative stimuli. Furthermore, a relevant source node of the network was represented by the PCC/PCu, which may be interpreted as corresponding to its central role in emotion formation and processing. Nevertheless,

we should also consider that in closed-eye condition α rhythms usually represent the main frequency of EEG activity [62]. Consequently, they may reflect also other processes not strictly related to the emotional regulation. Although it is out of the scope of this work, an interesting avenue for future studies may consider whether there is a relationship between the duration of cortical responses to odors and their frequency content. In this context, we advance the hypothesis that some of the interactions observed in the β band could be related to the hedonic amplitude of stimuli, independently of the direction. Indeed, during stimulation, several patterns of interactions were shared in the response to both positive and negative stimuli, but not to the neutral one.

The time-range in which connectivity analysis was carried out was determined through a GFP analysis. Specifically, we observed that around stimulus administration GFP was lower with respect to the resting baseline. Hence, we limited the analysis to a time span covering from rest $(-5,0)$s to post-stimulus (5,10)s. In particular, we assumed lower values of GFP would have been associated with a lower synchronization of global activity [63]. In this view, we hypothesized that during these time-windows lagged interactions among brain regions, instead of global synchronization, may occur. Accordingly, we investigated the presence of lagged interactions with MVAR models. Of note, the window for which we observe a first variation in GFP is the one covering from -1 s to 4 s around stimulus presentation. In this view, we can assume that the significant variation is due to the amount of post-stimulus data in such sliding window (i.e. 80%).

The physiological plausibility of the frequency ranges involved in the interactions and brain regions involved in the phenomenon suggest that the proposed approach can depict olfaction-related cortico-cortical interactions even in the presence of methodological challenges given by single-trial stimulation and limited timing control of the stimuli (i.e. without the use of an olfactometer). In particular, we exploited a moving-window approach with overlapping windows aiming at a smoothing the responses after stimulus administration. Furthermore, we used sufficiently-long windows to properly estimate MVAR model parameters in the case of single trials. Specifically, we controlled the window-length in relation to the number of sources and to the model order to obtain robust model estimates [22]. In this view, the proposed pipeline could be applied to more realistic situations such as ecological and/or social scenarios in which controlling the timing of olfactory stimuli as well as their number may be not possible.

The proposed pipeline of analysis was purposely developed to deal with single-trial stimuli. In particular, a specific issue concerns the limited SNR of the modelled timeseries that may increase the false positives and false negatives of the observed causalities [64]. Here, we attempted at maximizing the SNR of the available data with a multi-step procedure involving PCA and ICA analysis at single subject level, data cleaning by experts and subsequent clustering of components at the group level. Specifically, these multivariate approaches can lead to an improvement of SNR when artefact related components are detected and removed [65, 66]. In such procedure, a critical issue may be that of removing brain-related ICs, or conversely, maintaining artefact related ICs. Indeed, in both situations, an increase in false positives and/or false negatives may occur. In this scenario, the performed group-level clustering of independent components may reduce such risks by enhancing consistency of activity across different subjects [67]. Specifically, clustering ICs at the group level highlights common behaviours across subjects. Accordingly, clustered components are unlikely to be related to artefacts, that should be instead different across the subjects. As a result, the contribution of artefact-related components on the results is likely to be reduced.

Another limitation is related to the stimulation protocol, as it could be intrinsically characterized by limited standardization such as little differences in the distance between the vials and the nose. Accordingly, despite we cannot exclude that odors can potentially be perceived with slightly different intensities, they all were perceived equally in terms of arousal according to SAM test. In this view, since odor intensity has been positively correlated with subjective arousal such that odors that are more intense are rated as more arousing [68, 69], we hypothesized such differences as negligible.

We did not give any particular instructions to our participants regarding sniffing, in line with the notion that natural breathing patterns optimize odor detection [70]. However, since the presence of odors in the inhaled air changes sniffing patterns [71] and because smelling and sniffing both activate the brain, we cannot exclude that some of the observed differences in brain activation patterns are caused by condition dependent sniffing behavior that may not be captured by respiratory frequency alone. Future studies should carefully control for this variable.

We are aware that also faster dynamics are involved in olfaction, as for instance those observed with olfactory ERP [21]. In this context, the constraints for obtaining stable estimates of the MVAR model [22, 44] may represent a limitation for observing such dynamics in the single-trial case. Indeed, we had a lower bound on the window length (i.e. at least 6.5 s) mainly related to single-trial paradigm. Nevertheless, extending our pipeline to olfactory ERP paradigms would allow to resolve cortico-cortical interactions at smaller scales. In particular, the promising results in terms of observed interactions poses interesting insights for future

analysis of olfactory ERPs by means of connectivity methods. In such scenario, the use of a computer-controlled olfactometer would be unavoidable to properly control the stimulation times as well as the flow properties required for inducing olfactory ERPs [11, 20, 21].

Another limitation may be related to the tag of brain regions contributing to the network. Indeed, these regions were labelled based on the position of each cluster centroid. However, although the electrodes were placed in the same standard positions across the subjects through a geodesic net, we cannot exclude possible slight inaccuracies in source position estimation [72]. Another approximation is introduced by estimating dipole positions within the MNI template [73, 74]. Accordingly, from a physiological point of view, future improvements could consider a combination with other kind of data, as for instance MRI and fMRI, enabling a more detailed spatial description of brain areas.

A general limitation that should be considered when using EEG to study olfaction is related to the deepness of some of the structures involved in olfactory processing. Among these, the piriform cortex (PC), i.e. the primary olfactory cortex, is a deep structure in the brain. Moreover, other structures involved in olfaction, such as the amygdala (AM) and hippocampus (HIP) are even deeper [75–77]. Accordingly, the activity recorded with EEG is more likely to derive from projections of these brain areas onto the cortex rather than from their direct activation. In this context, the PC shows an extensive network of interconnections with cortical areas such as the orbitofrontal cortex (OFC) and the entorhinal cortex, as well as with subcortical regions. Here, we attempted at observing the cascade of events that followed olfactory stimulation in terms of cortico-cortical causal interactions. However, for investigating more deep structures, the integration of EEG with other techniques such as fMRI may be necessary.

The validity of asymmetrical causal interactions was assessed by rigorous statistical procedure of RPDC null distribution and by the validation of fitted MVAR models. Specifically, models were found to capture more than the 91% of correlation structure present in the data, according to the consistency analysis. However, a small portion of total dynamics may be represented by nonlinear interactions [44]. Although the fraction of non-captured dynamics is relatively small (i.e. 10%), future enhances in the model could include the presence of nonlinear interactions within the model parameters.

Data availability statement

The data that support the findings of this study are available upon reasonable request from the authors.

Acknowledgments

The research leading to these results has received partial funding from the Italian Ministry of Education and Research (MIUR) in the framework of the CrossLab project (Departments of Excellence). This research has received partial funding from European Union Horizon 2020 Programme under grant agreement n 824153 of the project 'POTION-Promoting Social Interaction through Emotional Body Odours'.

Conflict of interest statement

The authors declare no conflict of interest.

ORCID iDs

Alejandro Luis Callara https://orcid.org/0000-0003-2767-0699
Alberto Greco https://orcid.org/0000-0002-4822-5562
Johannes Frasnelli https://orcid.org/0000-0002-8863-3982
Gianluca Rho https://orcid.org/0000-0002-9919-9261
Nicola Vanello https://orcid.org/0000-0002-2312-6699
Enzo Pasquale Scilingo https://orcid.org/0000-0003-2588-4917

References

[1] Rolls E T 2004 The functions of the orbitofrontal cortex *Brain Cognit.* **55** 11–29
[2] Rolls E T and Grabenhorst F 2008 The orbitofrontal cortex and beyond: from affect to decision-making *Progress Neurobiol.* **86** 216–44
[3] Schultz W 2000 Reward processing in primate orbitofrontal cortex and basal ganglia *Cerebral Cortex* **10** 272–83
[4] Rolls E T, Kringelbach M L and de Araujo IET 2003 Different representations of pleasant and unpleasant odours in the human brain *Eur. J. Neurosci.* **18** 695–703
[5] Winston J S 2005 Integrated neural representations of odor intensity and affective valence in human amygdala *J. Neurosci.* **25** 8903–7
[6] Gottfried J A, Winston J S and Dolan R J 2006 Dissociable codes of odor quality and odorant structure in human piriform cortex *Neuron* **49** 467–79
[7] Jin J, Zelano C, Gottfried J A and Mohanty A 2015 Human amygdala represents the complete spectrum of subjective valence *J Neurosci.* **35** 15145–56
[8] Gottfried J A, Deichmann R, Winston J S and Dolan R J 2002 Functional heterogeneity in human olfactory cortex: an event-related functional magnetic resonance imaging study *J. Neurosci.* **22** 10819–28
[9] Li W, Howard J D, Parrish T B and Gottfried J A 2008 Aversive learning enhances perceptual and cortical discrimination of indiscriminable odor cues *Science* **319** 1842–5
[10] Schriever V A, Han P, Weise S, Hösel F, Pellegrino R and Hummel T 2017 Time frequency analysis of olfactory induced EEG-power change *PLoS One* **12** e0185596

[11] Lundström J N, Seven S, Olsson M J, Schaal B and Hummel T 2006 Olfactory event-related potentials reflect individual differences in odor valence perception *Chem. Senses* **31** 705–11

[12] Olofsson J K 2014 Time to smell: a cascade model of human olfactory perception based on response-time (RT) measurement *Front. Psychol.* **5** 1-8/33

[13] Goebel R and Linden D 2014 *Neurofeedback with Real-Time Functional MRI* ed C Mulert and M E Shenton (*MRI in Psychiatry*) (Berlin, Heidelberg: Springer) pp 35–46

[14] Moll J 2014 Voluntary enhancement of neural signatures of affiliative emotion using fMRI neurofeedback *PLoS One* **9** 1–11

[15] Li Z 2016 Self-regulating positive emotion networks by feedback of multiple emotional brain states using real-time fMRI *Exp. Brain Res.* **234** 3575–86

[16] Blinowska K J 2011 Review of the methods of determination of directed connectivity from multichannel data *Med. Biol. Eng. Comput.* **49** 521–9

[17] Pagnotta M F and Plomp G 2018 Time-varying MVAR algorithms for directed connectivity analysis: critical comparison in simulations and benchmark EEG data *PLoS One* **13** e0198846

[18] Pievani M, Filippini N, van den Heuvel M P, Cappa S F and Frisoni G B 2014 Brain connectivity in neurodegenerative diseases—from phenotype to proteinopathy *Nat. Rev. Neurol.* **10** 620–33

[19] Zhang H, Chavarriaga R, Goel M K, Gheorghe L and Milláan JdR 2012 Improved recognition of error related potentials through the use of brain connectivity features *2012 Annual Int. Conf. IEEE Engineering in Medicine and Biology Society* pp 6740–3

[20] Lundström J N, Gordon A R, Alden E C, Boesveldt S and Albrecht J 2010 Methods for building an inexpensive computer-controlled olfactometer for temporally-precise experiments *Int. J. Psychophysiol.* **78** 179–89

[21] Hummel T and Kobal G 2001 Olfactory event-related potentials *Methods and Frontiers in Chemosensory Research* (Boca Raton, FL: CRC) pp 429–64

[22] Schlögl A and Supp G 2006 Analyzing event-related EEG data with multivariate autoregressive parameters *Progress Brain Res.* **159** 135–47

[23] Stevenson R J and Wilson D A 2007 Odour perception: an object-recognition approach *Perception* **36** 1821–33

[24] Abbasi N I 2020 Decoding olfactory cognition: EEG functional modularity analysis reveals differences in perception of positively-valenced stimuli *Int. Conf. on Neural Information Processing* (Springer) pp 79–89

[25] Bell A J and Sejnowski T J 1995 An information-maximization approach to blind separation and blind deconvolution *Neural Comput.* **7** 1129–59

[26] Lütkepohl H 2005 *New Introduction to Multiple Time Series Analysis* 1 (Berlin: Springer Science & Business Media) XXI, 764 Google-Books-ID: COUFCAAAQBAJ

[27] Callara A L 2020 Ld-EEG effective brain connectivity in patients with cheyne-stokes respiration *IEEE Trans. Neural syst. Rehabil. Eng.* **28** 1216–25

[28] Oostenveld R, Fries P, Maris E and Schoffelen J M 2011 FieldTrip: open source software for advanced analysis of MEG, EEG and invasive electrophysiological data *Comput. Intell. Neurosci.* **2011** 1–9

[29] Schelter B, Timmer J and Eichler M 2009 Assessing the strength of directed influences among neural signals using renormalized partial directed coherence *J. Neurosci. Methods* **179** 121–30

[30] Skrandies W 1990 Global field power and topographic similarity *Brain Topography* **3** 137–41

[31] Frasnelli J, Lundström J N, Schöpf V, Negoias S, Hummel T and Lepore F 2012 Dual processing streams in chemosensory perception *Front. Hum. Neurosci.* **6** 288

[32] Georgiopoulos C 2018 Olfactory fMRI: implications of stimulation length and repetition time *Chem. Senses* **43** 389–98

[33] Sun X, Veldhuizen M G, Babbs A E, Sinha R and Small D M 2016 Perceptual and brain response to odors is associated with body mass index and postprandial total ghrelin reactivity to a meal *Chem. Senses* **41** 233–48

[34] Bradley M M and Lang P J 1994 Measuring emotion: the self-assessment manikin and the semantic differential *J. Behav. Therapy Exp. Psychiatry* **25** 49–59

[35] Naudin M, El-Hage W, Gomes M, Gaillard P, Belzung C and Atanasova B 2012 State and trait olfactory markers of major depression *PLoS One* **7** e46938

[36] Delorme A and Makeig S 2004 EEGLAB: an open source toolbox for analysis of single-trial EEG dynamics including independent component analysis *J. Neurosci. Methods* **134** 9–21

[37] Florin E, Gross J, Pfeifer J, Fink G R and Timmermann L 2010 The effect of filtering on Granger causality based multivariate causality measures *NeuroImage* **50** 577–88

[38] Mullen T R 2015 Real-time neuroimaging and cognitive monitoring using wearable dry EEG *IEEE Trans. Biomed. Eng.* **62** 2553–67

[39] Chang C Y, Hsu S H, Pion-Tonachini L and Jung T P 2018 Evaluation of artifact subspace reconstruction for automatic EEG artifact removal *2018 40th Annual Int. Conf. IEEE Engineering in Medicine and Biology Society (EMBC)* pp 1242–5

[40] Palmer J A, Kreutz-Delgado K, Makeig S, 2011, AMICA: an adaptive mixture of independent component analyzers with shared components 16

[41] Delorme A, Palmer J, Onton J, Oostenveld R and Makeig S 2012 Independent EEG sources are dipolar *PLoS One* **7** 2

[42] Onton J, Westerfield M, Townsend J and Makeig S 2006 Imaging human EEG dynamics using independent component analysis *Neurosci. Biobehav. Rev.* **30** 808–22

[43] Kaufman L and Rousseeuw P J 2009 *Finding Groups in Data: An Introduction to Cluster Analysis* (New York: Wiley) Google-Books-ID: YeFQHiikNo0C

[44] Courellis H, Mullen T, Poizner H, Cauwenberghs G and Iversen J R 2017 EEG-based quantification of cortical current density and dynamic causal connectivity generalized across subjects performing BCI-monitored cognitive tasks *Front. Neurosci.* **11** 180

[45] Ding M, Bressler S L, Yang W and Liang H 2000 Short-window spectral analysis of cortical event-related potentials by adaptive multivariate autoregressive modeling: data preprocessing, model validation and variability assessment *Biol. Cybern.* **83** 35–45

[46] Benjamini Y and Yekutieli D 2001 The control of the false discovery rate in multiple testing under dependency *Ann. Stat.* **29** 1165–88

[47] Theiler J, Eubank S, Longtin A, Galdrikian B and Doyne Farmer J 1992 Testing for nonlinearity in time series: the method of surrogate data *Physica* D **58** 77–94

[48] Storey J D and Tibshirani R 2003 Statistical significance for genomewide studies *Proc. Natl Acad. Sci.* **100** 9440–5

[49] Delorme A 2011 EEGLAB, SIFT, NFT, BCILAB and ERICA: new tools for advanced EEG processing *Comput. Intell. Neurosci.* **2011** 1–12

[50] Bonnì S 2015 TMS evidence for a selective role of the precuneus in source memory retrieval *Behav. Brain Res.* **282** 70–5

[51] Phillips M L 1998 Investigation of facial recognition memory and happy and sad facial expression perception: an fMRI study *Psychiatry Res.: Neuroimaging* **83** 127–38

[52] Rempel-Clower N L 2007 Role of orbitofrontal cortex connections in emotion *Ann. New York Acad. Sci.* **1121** 72–86

[53] Lorig T S and Schwartz G E 1988 Brain and odor: I. Alteration of human EEG by odor administration *Psychobiology* **16** 281–4

[54] Royet J P, Plailly J, Delon-Martin C, Kareken D A and Segebarth C 2003 fMRI of emotional responses to odors:: influence of hedonic valence and judgment, handedness and gender *NeuroImage* **20** 713–28

[55] Frank D W, Costa V D, Averbeck B B and Sabatinelli D 2019 Directional interconnectivity of the human amygdala, fusiform gyrus and orbitofrontal cortex in emotional scene perception *J. Neurophysiol.* **122** 1530–7
[56] Maren S 1999 Long-term potentiation in the amygdala: a mechanism for emotional learning and memory *Trends Neurosci.* **22** 561–7
[57] Rolls E T 2005 Reward-spatial view representations and learning in the primate hippocampus *J. Neurosci.* **25** 6167–74
[58] Price J L 2010 *Connections of Orbital Cortex* (Oxford: Oxford University Press) pp 1–20
[59] Carmichael S T P J 1996 Connectional networks within the orbital and medial prefrontal cortex of macaque monkeys 29
[60] Martin G N 1998 Human electroencephalographic Ž EEG response to olfactory stimulation: two experiments using the aroma of food 16
[61] Zhao G, Zhang Y and Ge Y 2018 Frontal EEG asymmetry and middle line power difference in discrete emotions *Front. Behav. Neurosci.* **12**
[62] Tatum W O 2013 *Handbook of EEG Interpretation* (New York: Demos Medical Publication) 2013 OCLC: 841495449
[63] Brunet D, Murray M M and Michel C M 2011 Spatiotemporal analysis of multichannel EEG: CARTOOL *Comput. Intell. Neurosci.* **2011**
[64] Bastos A M and Schoffelen J M 2016 A tutorial review of functional connectivity analysis methods and their interpretational pitfalls *Front. Syst. Neurosci.* **9**
[65] Jung T P 2000 Removing electroencephalographic artifacts by blind source separation *Psychophysiology* **37** 163–78
[66] Artoni F, Delorme A and Makeig S 2018 Applying dimension reduction to EEG data by principal component analysis reduces the quality of its subsequent independent component decomposition *NeuroImage* **175** 176–87
[67] Zeman P M, Till B C, Livingston N J, Tanaka J W and Driessen P F 2007 Independent component analysis and clustering improve signal-to-noise ratio for statistical analysis of event-related potentials *Clin. Neurophysiol.* **118** 2591–604
[68] Bensafi M, Rouby C, Farget V, Bertrand B, Vigouroux M and Holley A 2002 Autonomic nervous system responses to odours: the role of pleasantness and arousal *Chemi. Senses* **27** 703–9
[69] Liu Y, Toet A, Krone T, van Stokkum R, Eijsman S and van Erp J B 2020 A network model of affective odor perception *PLoS One* **15** e0236468
[70] Laing D G 1983 Natural sniffing gives optimum odour perception for humans *Perception* **12** 99–117
[71] Laing D G 1982 Characterisation of human behaviour during odour perception *Perception* **11** 221–30
[72] Dalal S S, Rampp S, Willomitzer F and Ettl S 2014 Consequences of EEG electrode position error on ultimate beamformer source reconstruction performance *Front. Neurosci.* 8
[73] Brodbeck V 2011 Electroencephalographic source imaging: a prospective study of 152 operated epileptic patients *Brain* **134** 2887–97
[74] Zanow F and Peters M J 1995 Individually shaped volume conductor models of the head in EEG source localisation *Med. Biol. Eng. Compt.* **33** 582–8
[75] Rolls E T 2019 Taste and smell processing in the brain *Handbook Clin. Neurol.* **164** 97–118
[76] Soudry Y, Lemogne C, Malinvaud D, Consoli S M and Bonfils P 2011 Olfactory system and emotion: common substrates *Eur. Ann. Otorhinolaryngol. Head Neck Diseases* **128** 18–23
[77] Bao X, Raguet L L, Cole S M, Howard J D and Gottfried J A 2016 The role of piriform associative connections in odor categorization *Elife* **5** e13732